Remote Sensing of Environment 287 (2023) 113466

Contents lists available at ScienceDirect

Remote Sensing of Environment

journal homepage: www.elsevier.com/locate/rse

Time series soil moisture retrieval from SAR data: Multi-temporal constraints and a global validation

Liujun Zhu [a,b], Shanshui Yuan [a,*], Yi Liu [c], Cheng Chen [d], Jeffrey P. Walker [b]

[a] Yangtze Institute for Conservation and Development, Hohai University, Nanjing 210098, China
[b] Department of Civil Engineering, Monash University, Clayton, Vic 3800, Australia
[c] College of Hydrology and Water Resources, Hohai University, Nanjing 210098, China
[d] State Key Laboratory of Hydrology-Water Resources and Hydraulic Engineering, Nanjing Hydraulic Research Institute, Nanjing 210029, China

ARTICLE INFO

Edited by Jing M. Chen

Keywords:
Soil moisture
Synthetic aperture radar
Multi-temporal
Global validation

ABSTRACT

Time series algorithms for soil moisture retrieval from synthetic aperture radar (SAR) data have steadily increased in popularity over the past decade due to the feasibility of decoupling the effect of other surface variables, and the increasing availability of dense time series SAR data. While soil moisture inversion from time series data can utilize more independent observations, the value of further constraints on the inversion process are widely acknowledged. However, how to constrain a time series retrieval for global soil moisture mapping is still unresolved. In this study, three kinds of time series constraints were further developed and evaluated, including the use of 1) temporal behavior of soil moisture and soil moisture bounds; 2) temporal behavior of vegetation or time-invariant vegetation; and 3) time series ensemble skill. The effect of these constraints was investigated using 4 years (2016–2019) C-band Sentinel-1 data collected over 547 worldwide stations from 17 networks available on the international soil moisture network (ISMN) and intensive ground samples collected during the Fifth Soil Moisture Active and Passive Experiment (SMAPEx-5). While the effect of these temporal retrieval skills varies in time and space, the global validation yielded four general suggestions: 1) the assumption of time-invariant vegetation contributed negatively even for a short retrieval period of $\leq$12 days; 2) reliable soil moisture bounds of each retrieval period can substantially improve the retrieval statistics at the cost of an underestimated soil moisture range; 3) the temporal constraints of soil moisture and vegetation need to be used together with the soil moisture bounds for reliable estimation; 4) the use of an ensemble retrieval could partly remove the retrieval uncertainties at the expense of underestimating soil moisture variation. The use of these constraints resulted in a competitive correlation coefficient (R: 0.64), root mean square error (RMSE: 0.072 m^3/m^3) and unbiased RMSE (ubRMSE: 0.052 m^3/m^3) at a spatial grid of 100 m, with similar performance achieved across a retrieval window up to 132 days.

1. Introduction

Surface soil moisture (top 5 cm) is important for its impact on land-atmosphere interactions and its partitioning of rainfall into runoff through regulation of the infiltration capacity of the soil (Demargne et al., 2014). Economic, social and environmental planning for a water-limited future requires a capacity to monitor soil moisture content at a level of spatial (0.1–1 km) and temporal (< 3 days) detail that does not currently exist (Peng et al., 2020). Despite the modest retrieval accuracy, the recent investments in space-borne Synthetic Aperture Radars (SAR) enables access to massive free SAR data with an enhanced data revisit of a few days, e.g., the NASA-ISRO Synthetic Aperture Radar (NISAR, Kellogg et al., 2020), BIOMASS (Quegan et al., 2019), Sentinel-1 (Torres et al., 2012) and Chinese Terrestrial Water Resources Satellite (TWRS, Zhao et al., 2020), being an operational source of frequent global soil moisture mapping.

In the past four decades, great efforts have been made to retrieve soil moisture from SAR data (Kornelsen and Coulibaly, 2013). Most studies have focused on developing an "optimal" scattering model (Dubois et al., 1995; Oh, 2004; Shi et al., 1997) and/or inversion process for a specific retrieval scenario (see Kornelsen and Coulibaly, 2013 for a review). Various parameterization solutions of rough soil surfaces were proposed to account for the effect of roughness (e.g., Lievens et al., 2011; Zribi et al., 2014), which commonly includes 1–3 parameters (Fung,

* Corresponding author.
E-mail address: yuanshanshui@hhu.edu.cn (S. Yuan).

https://doi.org/10.1016/j.rse.2023.113466
Received 23 July 2022; Received in revised form 5 January 2023; Accepted 17 January 2023
Available online 25 January 2023

1994), e.g., the root mean square height, correlation length and their equivalents or invariants. Similarly, the complex vegetation layers were simplified and described as a few parameters, with the most famous parameterization being the water cloud (Attema and Ulaby, 1978). Based on these simplifications and/or parameterizations, the complex earth surface scattering can be modeled using a limited number of parameters (Chen et al., 2003; Fung, 1994; Gu et al., 2021; Huang and Tsang, 2012).

Despite the advances, soil moisture retrieval as an inversion process of the above models remains a challenge because of the large number of unknowns to be determined. Consequently, multi-angular (Baghdadi et al., 2006; Merzouki and McNairn, 2015; Rahman et al., 2008; Sahebi and Angles, 2010; Shi et al., 2021) and/or multi-frequency (Bindlish and Barros, 2000; Pierdicca et al., 2008; Zhu et al., 2019a) SAR data were used to introduce more independent observations. Moreover, *a prior* information has been used to constrain the inversion process, such as an initial guess of soil moisture and/or roughness values (Joseph et al., 2008; Mattia et al., 2009); the range, possibility and probability distributions of soil moisture and roughness (Pierdicca et al., 2008; Verhoest et al., 2007; Vernieuwe et al., 2010). Various ancillary data have also been used to constrain the retrieval or as inputs of scattering models. Soil moisture from coarse passive microwave data and hydrological models were confirmed to be an effective guess of high-resolution soil moisture (Kim and Van Zyl, 2009; Mattia et al., 2006; Mattia et al., 2009; Zhan et al., 2006), while optical data (e.g., Landsat series and Sentinel-2) and passive data have been widely used as a source of vegetation information required in vegetation scattering models (Bousbih et al., 2018; El Hajj et al., 2016; Wang et al., 2021b).

The use of time series SAR data provides a promising alternative to address the problem of ill-posed inversion. This so-called change detection technique assumes that the vegetation canopy and soil roughness change little in the retrieval period, and thus directly relates the variation of backscatter to that of soil moisture (Balenzano et al., 2011; Ouellette et al., 2017; Wagner et al., 1999a; Wagner et al., 1999b; Zribi et al., 2020; Zribi et al., 2007). The snapshot methods used to inverse a scattering model have been similarly extended for time series data with the roughness and/or vegetation being assumed time-invariant (Fan et al., 2021; Kim et al., 2014; Kim et al., 2012; Mattia et al., 2009; Zhu et al., 2019b). These multi-temporal algorithms have been increasingly popular in the past decade because of: 1) the simplicity of decoupling the effect of soil moisture and other surface variables; 2) the increasing availability of dense time series data; and 3) the convenience to retrieve soil moisture over a large spatial area (Balenzano et al., 2021; Bauer-Marschallinger et al., 2018).

The challenge is that more observations also mean more unknowns and so the uncertainties are not fully addressed (Ulaby et al., 2014; Zhao et al., 2021). Moreover, a globally well calibrated forward scattering model is not available due to the absence of extensive ground roughness and vegetation samples, with only the SMAP radar baseline algorithm used to model L-band backscattering globally (Kim et al., 2014). This means large scale soil moisture retrieval from SAR data can only use imperfect scattering models with large uncertainties. Consequently, constraining the inversion process with *a prior* information and ancillary data still plays an important role in time series algorithms. An accurate guess of maximum and minimum soil moisture is key to the performance of short-term change detection methods (Ouellette et al., 2017; Palmisano et al., 2020) and empirical relationships (Kim and Van Zyl, 2009), while an assumption of dry down soil moisture for a period after a rainfall can substantially improve the retrieval accuracy (Zhu et al., 2019a, 2019b). The knowledge of temporal vegetation and roughness variation is critical for determining a proper retrieval time window (Zhu et al., 2019a).

In contrast to the snapshot methods with numerous studies on inversion constraints and skills, how best to constrain the inversion of time series retrieval remains unresolved. Consequently, the aforementioned soil moisture and vegetation constraints were further developed using common auxiliary data and evaluated independently and collectively for an improved time series retrieval, including the use of 1) temporal behavior of soil moisture and the soil moisture bounds; 2) temporal behavior of vegetation or time-invariant vegetation; and 3) time series ensemble skills. These constraints were treated as extensions of the time series retrieval algorithm of (Zhu et al., 2020), being also compatible with other model based time series methods. The in-situ soil moisture collected from 547 worldwide stations available on the international soil moisture network (ISMN, Dorigo et al., 2021) and the ground samplings made in the Fifth Soil Moisture Active and Passive Experiment (SMAPEx-5, Ye et al., 2020) were used as the ground truth. The effects of these constraints on soil moisture retrieval were investigated using time series C-band Sentinel-1 data, being expected to provide some straightforward principles on how to constrain scattering-model based time series inversion.

2. Methodology

2.1. Time series retrieval scheme

The time series retrieval scheme used in this study was built on the stochastic ensemble inversion method (Zhu et al., 2020) and the concept of using sliding window processing (Balenzano et al., 2021) for operational soil moisture mapping. Given a Sentinel-1 acquisition k, it was processed together with the previous $N_t - 1$ acquisitions (e.g., $N_t = 4$ in Fig. 1). The N_e sub-time-series were then randomly generated from the original VV and HV Sentinel-1 data with random polarization combinations, resulting in N_e sub-retrievals for each time instance ($N_e = 2$ in Fig. 1). The sliding window was then moved forward to retrieve the soil moisture of the following time instances. Consequently, there were $N_t \times N_e$ retrievals for each time instance except the first and last N_t - 1 time instances, which were ensemble averaged as the output. The multiple sub-retrievals with different inputs are expected to improve the retrieval accuracy by reducing the effect of uncertainties (Lee et al., 2021; Zhu et al., 2020). The parameter of N_e was set to 10 in this study according to the sensitivity analysis of Zhu et al. (2020), with the special case of $N_e = 1$ being the single retrieval using all the input data (i.e., time series VV and VH for Sentinel-1).

In each sub-retrieval, N_t soil moisture values were achieved by minimizing:

$$f_\sigma = \sum_{i=1}^{N_t} \sqrt{\frac{1}{N_i} \sum_{j=1}^{N_i} \left(\sigma_{ij}^0 - \sigma_{\mathrm{model},ij}^0 (S_i, V_i, mv_i) \right)} \quad (1)$$

where subscript i refers to the ith acquisition within the sliding window and N_i is the number of selected polarizations from the ith acquisition, being 1 or 2 for Sentinel-1. $\sigma_{\mathrm{model},ij}^0$ and σ_{ij}^0 are the modeled and observed backscattering coefficients in dB respectively, with the S_i, V_i, and mv_i being the soil surface roughness parameters, vegetation parameters, and soil moisture.

In this study, look up tables (LUTs) built by the Oh model (Oh, 2004) and the distorted Born approximation (DBA, Lang and Sighu, 1983) were used to present the scattering of bare soil and vegetated area (Zhu et al., 2019a). Only one independent roughness parameter was considered, being the root mean square (s) height ranging from 0.5 to 4 cm. The vegetation was approximated as a layer of randomly distributed cylinders and the vegetation parameters required in the DBA were all collected in SMAPEx-5. These vegetation parameters were all related to vegetation water content (VWC) using allometric relationships. The VWC and mv of LUTs ranged from 0 to 4 kg/m^2 and 0.03 to 0.47 m^3/m^3 respectively. Evaluation based on C-band RADARSAT-2 data showed an RMSE of $<$2.2 dB on three general landcover types (bare soil, wheat and grass), with consistent performance for an incidence angle of 22.4–39.5° (Zhu et al., 2019a). Since soil surface roughness in agricultural areas has shown negligible variation from tens days to a whole crop season after

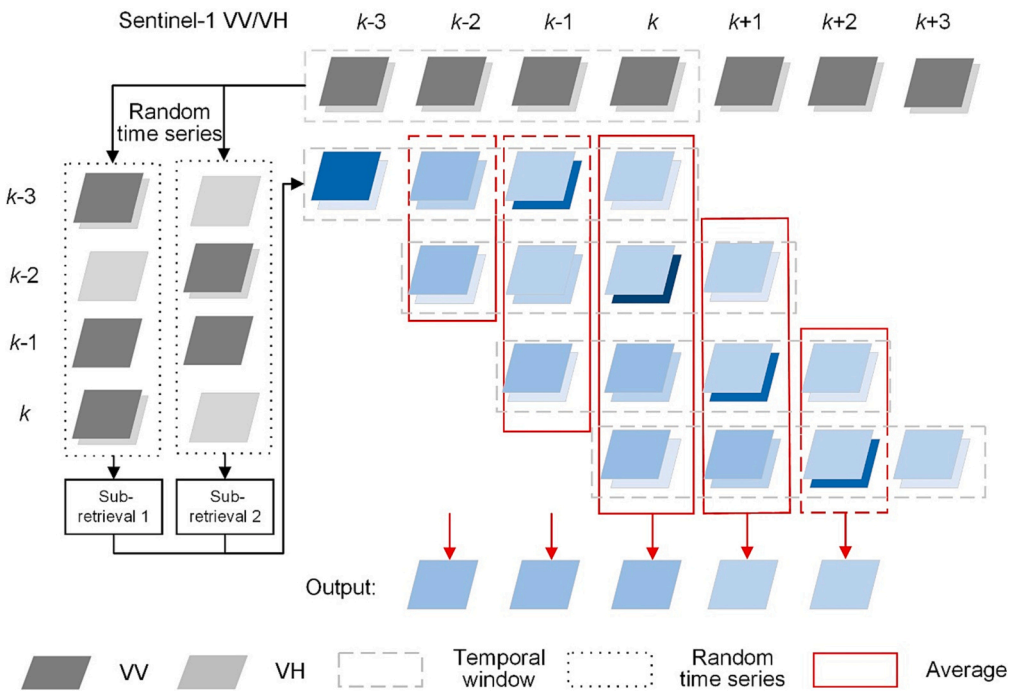

Fig. 1. The retrieval scheme for time series soil moisture maps: a sliding window (e.g., $N_t = 4$) was used to determine the input time series data; an ensemble (e.g., $N_e = 2$) of sub-series were arbitrarily selected with random polarization combinations; soil moisture was retrieved independently using each sub-series. The sliding window was moved forward, resulting in $N_t \times N_e$ soil moisture maps at each time instance k except the first and last $N_t - 1$ instances. The soil moisture maps were averaged for each time instance as the output.

soil tillage (Callens et al., 2006; Njoku et al., 2002; Ye et al., 2020), Eq. (1) becomes:

$$f_\sigma = \sum_{i=1}^{N_t} \sqrt{\frac{1}{N_i}\sum_{j=1}^{N_i}\left(\sigma_{ij}^0 - \sigma_{\text{model},ij}^0(s, \text{VWC}_i, mv_i)\right)} \quad (2)$$

with $2N_t + 1$ unknowns and N_t to $2N_t$ independent observations for each sub-retrieval, being still ill-posed. Therefore, more constraints about vegetation and soil moisture are still required for a stable solution.

2.2. Vegetation constraints

In general, vegetation has seasonal variation and undergoes smooth evolution in time. The periodic variation can be modeled to relate the vegetation dynamic and σ^0 changes, being either used to correct the time series σ^0 (Pierdicca et al., 2010) or integrated into the long-term change detection algorithms (Wagner et al., 1999a). Vegetation indices, e.g., the Normalized Difference Vegetation Index (NDVI), were commonly used to provide the vegetation dynamic. Despite the success of these relationships, the vegetation dynamic cannot be directly integrated into the proposed multi-temporal inversion scheme because existing vegetation scattering models and Eq. (2) are not compatible with such information. Alternatively, Kim et al. (2017) estimated VWC climatology using time series NDVI and took the retrieved VWC values as the inputs of a cost function like Eq. (2). Reliable estimation of VWC climatology however is as challenging as the soil moisture retrieval.

In contrast, the existing short-term multi-temporal methods assume time-invariant vegetation for a short retrieval window (Balenzano et al., 2011; He et al., 2017; Ouellette et al., 2017; Zhu et al., 2019b), resulting in:

$$\text{VWC}_1 = \text{VWC}_2 = \ldots = \text{VWC}_{N_t} \quad (3)$$

Eq. (2) thus becomes well-constrained at the expense of introducing extra uncertainties from the potential vegetation changes. Although most of these studies were confined to a short retrieval period of 1–5 weeks (2–8 Sentinel-1 acquisitions), substantial VWC changes can occur with their impact on retrieval being unclear. Apart from investigating the effect of VWC temporal variation, a "soft" variant of Eq. (3) was proposed in this study, inspired by the modelling of vegetation dynamics. Given any two time-instances i and j with $\text{NDVI}_i \leq \text{NDVI}_j$, the VWC_i and VWC_j in Eq. (2) was forced to meet:

$$\text{VWC}_{\min} \leq \text{VWC}_i \leq \text{VWC}_j \leq \text{VWC}_{\max}, i, j \in (1, 2, \ldots, N_t) \quad (4)$$

where $\text{VWC}_{\min}$ and $\text{VWC}_{\max}$ were taken as 0 and 4 kg/m^2 respectively, being consistent with the bounds of LUTs. Eq. (4) is a safer but weaker constraint compared to Eq. (3), because the time-invariant vegetation is replaced by observed vegetation evolutions but N_t unknows of VWC need to inverted from Eq. (2).

2.3. Soil moisture constraints

The most widely used soil moisture constraint is the minimum and maximum soil moisture of the retrieval scenario. While the range of soil moisture can vary substantially across a watershed, a fixed minimum value (e.g., 0.03 m^3/m^3) and/or a maximum value (e.g., 0.5 or 0.6 m^3/m^3) have been commonly applied (Balenzano et al., 2021; Zhu et al., 2022). Such bounds have been either used to constrain the numerical inversion of scattering models or used as the bounds of LUTs. Since the soil moisture range of the LUTs was 0.03–0.47 m^3/m^3, Eq. (2) includes an inherent constraint of:

$$0.03 \leq mv_i \leq 0.47 \quad (5)$$

Obviously, this can substantially overestimate the range of soil moisture for dry and/or wet seasons, with many studies reporting the importance of an accurate soil moisture bound for short-term change detection methods (Al-Khaldi et al., 2019; Balenzano et al., 2021; He et al., 2017; Ouellette et al., 2017; Zhu et al., 2022). Consequently, its effect on scattering-model-based methods (Eq. (2)) was investigated in this study. The sophisticated coarse resolution passive microwave data and hydrological models can provide an effective guess of soil moisture in regional soil moisture retrieval (Kim and Van Zyl, 2009; Mattia et al., 2006; Mattia et al., 2009; Zhan et al., 2006), with the SMAP L3 passive product (36 km) being used in this study considering its relatively better accuracy than other coarse resolution soil moisture products (Cui et al., 2017; Wang et al., 2021a). Given a retrieval time window of k to $k + N_t$, all of the SMAP soil moisture products collected were used to determine

the:

$$mv_{\min} = min\left(mv_i^{\mathrm{SMAP}}, \ldots, mv_j^{\mathrm{SMAP}}, mv_{\mathrm{ave}}^{\mathrm{SMAP}}\right), k \le i \le j \le k + N_t \quad (6)$$

$$mv_{\max} = max\left(mv_i^{\mathrm{SMAP}}, \ldots, mv_j^{\mathrm{SMAP}}, mv_{\mathrm{ave}}^{\mathrm{SMAP}}\right), k \le i \le j \le k + N_t \quad (7)$$

where $mv_{\mathrm{ave}}^{\mathrm{SMAP}}$ is the mean of all SMAP measurements of the corresponding retrieval area. Eq. (6) and Eq. (7) were demonstrated to estimate reliable soil moisture bounds in the Yanco area, Australia (Zhu et al., 2022).

Similar to the temporal constraint of vegetation (Eq. (4)), the soil moisture can be further constrained by the temporal evolution of the SMAP passive products. Given any two time-instances i and j with $mv_i^{\mathrm{SMAP}} \le mv_j^{\mathrm{SMAP}}$, the mv_i and mv_j in Eq. (2) was forced to meet:

$$mv_{\min} \le mv_i \le mv_j \le mv_{\max} \quad (8)$$

Since irrigation or small-scale rainfall events lead to different temporal variation of soil moisture within a SAMP passive grid, Eq. (8) was removed when $\sigma_i - \sigma_j \ge 1$ dB to avoid the exclusion of soil moisture "anomalies" (Zhu et al., 2022).

2.4. Inversion and evaluation methods

The main contribution of this study is a global validation of the potential constraints on multi-temporal soil moisture retrieval methods. A total of 4 constraints were presented above, with the time invariant VWC (Eq. 3) conflicting with the VWC trend (Eq. 4). Accordingly, 9 multi-temporal retrieval algorithms were considered as outlined in Table 1, and compared with their ensemble alternative (Fig. 1). Each algorithm invariant was expressed as four letters of T (True) and/or F (False) for simplification (Table 1), with the applied constraints labeled as T. For example, the algorithm without any constraint was labeled as FFFF.

Apart from the constraint of soil moisture bounds, the use of multiple other constraints results in a conventional multi-objective optimization problem, with some sophisticated algorithms available (Deb, 2014). However, a multi-objective optimization can be extremely time consuming, and thus was simplified as a single objective optimization by integrating the cost-function of vegetation (f_v) and/or soil moisture (f_{mv}) into Eq. 2:

$$F = f_\alpha f_V f_{mv} \quad (9)$$

$$f_V = \sum_{i=k}^{k+N_t} \left| r_{\mathrm{VWC},i} - r_{\mathrm{NDVI},i} \right| + 1 \quad (10)$$

$$f_{mv} = \sum_{i=k}^{k+N_t} \left| r_{mv,i} - r_{\mathrm{SMAP},i} \right| + 1 \quad (11)$$

where $r_{\mathrm{VWC},\,i}$, $r_{\mathrm{NDVI},\,i}$, $r_{mv,\,i}$, $r_{\mathrm{SMAP},\,i}$ are the order of ith VWC, NDVI, mv and SMAP soil moisture in the corresponding time series, respectively. f_V is 1 when the temporal trend of VWC completely matches that of NDVI, reaching the maximum value of $0.5N_t^2 + 1$ when the two trends are reversed. A genetic algorithm was used to find the optimal solution of Eq. 10 for time series soil moisture retrieval. The number of chromosomes and the maximum generation (iteration) required in the genetic algorithm was 30 and 100 respectively. The outputs of the 100th iteration were treated as the retrieved results regardless of the value of the cost function. The retrieval performance was evaluated using 4 widely used indicators including bias, correlation coefficient (R), root mean square error (RMSE) and unbiased RMSE (ubRMSE). The Student's t-test was used to check the significance of performance difference.

Table 1
Variants of the multi-temporal retrieval algorithm, with the applied constraint being labeled as True.

Algorithms	Time invariant VWC (Eq. 3)	VWC trend (Eq. 4)	mv bound (Eq. 6 and 7)	mv trend (Eq. 8)
TFFF	**True**	False	False	False
FFFF	False	False	False	False
FTFF	False	**True**	False	False
FFTF	False	False	**True**	False
FFFT	False	False	False	**True**
FFTT	False	False	**True**	**True**
FTTF	False	**True**	**True**	False
FTFT	False	**True**	False	**True**
FTTT	False	**True**	**True**	**True**

3. Data and preprocessing

3.1. Soil moisture

In this study, the soil moisture measurements available on the ISMN (Dorigo et al., 2021) were considered for validations. Since the forward LUTs were built on a single layer of random cylinders with a maximum VWC of 4 kg/m^2, only the stations over bare soil, grassland, cropland or shrubland were used. The Copernicus Global Land Cover Layers was used to provide the landcover type of each station (Buchhorn et al., 2020). All the 2016–2019 recordings with a sensing depth $\le$ 5 cm were downloaded using the ISMN batch service (Dorigo et al., 2021). The Shuttle Radar Topography Mission Digital Elevation Data Version 3 (SRTM DEM V3) was used to calculate the slope of each station, with these having a slope of $>5^\circ$ being removed, considering the challenging of terrain correction and flattening. Moreover, only high-quality recordings were used, being these with a flag of "G".

As the measuring depths of shallow surface soil moisture ($\le$ 5 cm) varied across networks (e.g., at 0–5 cm, 2 cm and/or 5 cm), they were treated as independent estimations of the $\le$5 cm soil moisture. Accordingly, all the recordings of a station collected within 5 cm was averaged as the daily averaged soil moisture. These beyond the LUTs (0.03–0.47 m^3/m^3) were then discarded. In order to get interpretable station-specific accuracy statistics, only the stations with $\ge$30 valid daily soil moisture measurements were used. After applying these filters, a total of 547 stations from 17 networks were used in this study (Table 2). Notably, the 34 OzNet stations were all located in the Yanco area, NSW, Australia (Fig. 2), being different from these in the ISMN.

Extensive soil moisture samples collected from a 5 $\times$ 20 km area of SMAPEx-5 (the red rectangle in Fig. 2) was also used. The campaign was conducted in the Yanco area, Australia, as part of the SMAP global Cal/Val scheme (Ye et al., 2020). The Yanco area is characterized as semiarid with an average annual precipitation of 300 mm. The soil texture is mainly clay to sandy soil, with the dominated land use being grazing and cropping. The vegetation type for grazing areas is natural grass, while the cropping area had seasonal transitions of crops and/or fallow (bare soil). The averaged soil moisture of all OzNet sites is depicted in Fig. 3, with clear inter-annual dry-wet cycle and droughts in 2018 and 2019.

Nearly concurrent soil moisture samples were collected during the acquisition dates of two Sentinel-1 images (Sep. 15 and 27), with the time difference being <20 h. These soil moisture samples were made on an east-west oriented grid using the Hydraprobe sensor (Merlin et al., 2007), with three replicate soil moisture readings of 0–5 cm at each plot (Fig. 2). Similarly, measurements <0.03 or > 0.47 m^3/m^3 were discarded, with a total of 566 valid samples. Other surface parameters, e.g., VWC, vegetation structure parameters and soil surface roughness, were also measured in this area (Ye et al., 2020) and were used in the parametrization and calibration of surface and vegetation scattering models (Zhu et al., 2019a).

3.2. Remote sensing data and preprocessing

The SMAP L3 passive soil moisture product (Version 6, Neill et al., 2019), Moderate Resolution Imaging Spectroradiometer (MODIS) NDVI

Table 2
the 17 soil moisture networks used for evaluation. The A/D in the orbit pass refers to the ascending/descending.

Network	# stations	# mv records	# orbits	Orbit pass	Average revisit (days)*	Incidence angle	Reference
AMMA-CATCH	5	474	1–2	A	5.2–12.4	31.0–44.7	(Galle et al., 2018)
ARM	15	2490	1–2	A	5.7–15.1	33.0–44.9	(Cook, 2016)
HOAL	18	4007	2	A/D	3.4–3.4	38.3–39.2	(Blöschl et al., 2016)
HOBE	21	5577	4	A/D	1.8–2.3	30.0–45.2	(Jensen and Refsgaard, 2018)
MAQU	11	376	2–3	A/D	6–12	32.8–46.1	(Su et al., 2011)
NAQU	9	795	3	A/D	6.1	31.5–45.2	(Su et al., 2011)
NGARI	15	1392	2–3	A/D	5.3–7.6	34.2–45.5	(Su et al., 2011)
OzNet	34	4080	1	D	12	35.3–40.0	(Smith et al., 2012)
PBO_H2O	94	4752	1–4	A/D	3.7–17	30.3–45.7	(Larson et al., 2008)
REMEDHUS	16	5556	2–3	A/D	3.2–6.1	30.5–42.1	(González-Zamora et al., 2019)
RISMA	23	2354	2–3	A/D	6–12	31.1–43.7	(Ojo et al., 2015)
RSMN	12	5678	2–4	A/D	1.7–3.3	30.2–45.1	
SCAN	127	16,814	1–4	A/D	4.5–16.5	30.4–45.6	(Schaefer et al., 2007)
SMN-SDR	27	1770	3–4	A/D	3.8–5.2	30.6–44.1	(Zhao et al., 2020)
SMOSMANIA	11	4931	2–4	A/D	2.2–3.9	30.5–45.4	(Calvet et al., 2016)
SOILSCAPE	35	449	2–3	A/D	5.7–6.1	30.8–43.4	(Moghaddam et al., 2016)
USCRN	74	10,055	1–4	A/D	3.5–16.5	30.4–45.6	(Bell et al., 2013)
Total	547	68,468					

* Average values for 2016–2019. The absence of a few acquisitions resulted in a revisit > the 12-day nominal revisit.

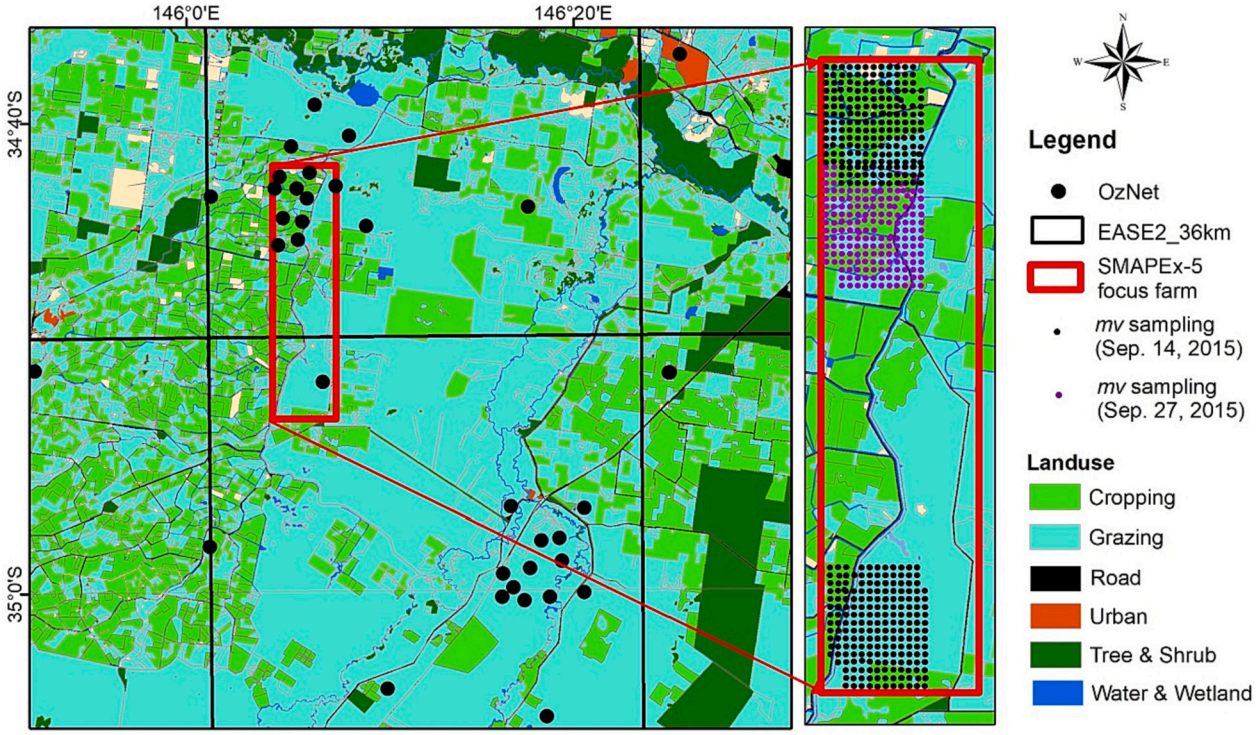

Fig. 2. The Yanco area and OzNet soil moisture stations as well as the SMAPEx-5 ground soil moisture samples collected nearly concurrently with the two Sentinel-1 acquisitions; Sep. 15 and Sep. 272,015.

products and Sentinel-1 Interferometric Wide (IW) ground range detected (GRD) products were used in this study. All the Sentinel-1 IW GRD acquisitions available on Google Earth Engine (GEE) were used in this study. The GEE Sentinel-1 GRD collection was produced by the Sentinel-1 Toolbox with the main steps including GRD border and thermal noise removal, radiometric calibration, and terrain correction (orthorectification). Radiometric terrain correction and flattening is not made because of the large uncertainty in the available DEM. The GRD data has two polarizations (VV and VH) and a spacing of 10 m. Since the IW data over a station can be collected from varying orbit passes (ascending/descending) and/or multiple relative orbits, the average revisit and the time interval between two successive acquisitions varied timely and spatially (Table 2). This means that the same N_t can have different lengths of retrieval widow in time across the 547 stations. The maximum time interval of two successive acquisitions was generally ≤12 days expect some short special periods without data. In this study, the GEE GRD data with a pixel size of 10 m was resampled to 100 m using the "reduceResolution" method provided by GEE (https://developers.google.com/earth-engine/guides/resample). In brief, the 10 m pixels were aggregated to larger pixels of 100 m on the Universal Transverse Mercator (UTM) local projection used in the Sentinel-1 data, e.g., the UTM 55S for the Yanco area. This is expected to substantially reduce the effect of speckle noise and result in a satisfactory radiometric accuracy of ~0.4 dB (Torres et al., 2012).

The Terra and Aqua MODIS vegetation indices products (MOD13Q1 and MYD13Q1, V6) were used to provide the time series NDVI required in Eq. 4. Since the two NDVI data sets were from two identical sensors, they were merged to an 8-day composite with an initial resolution of

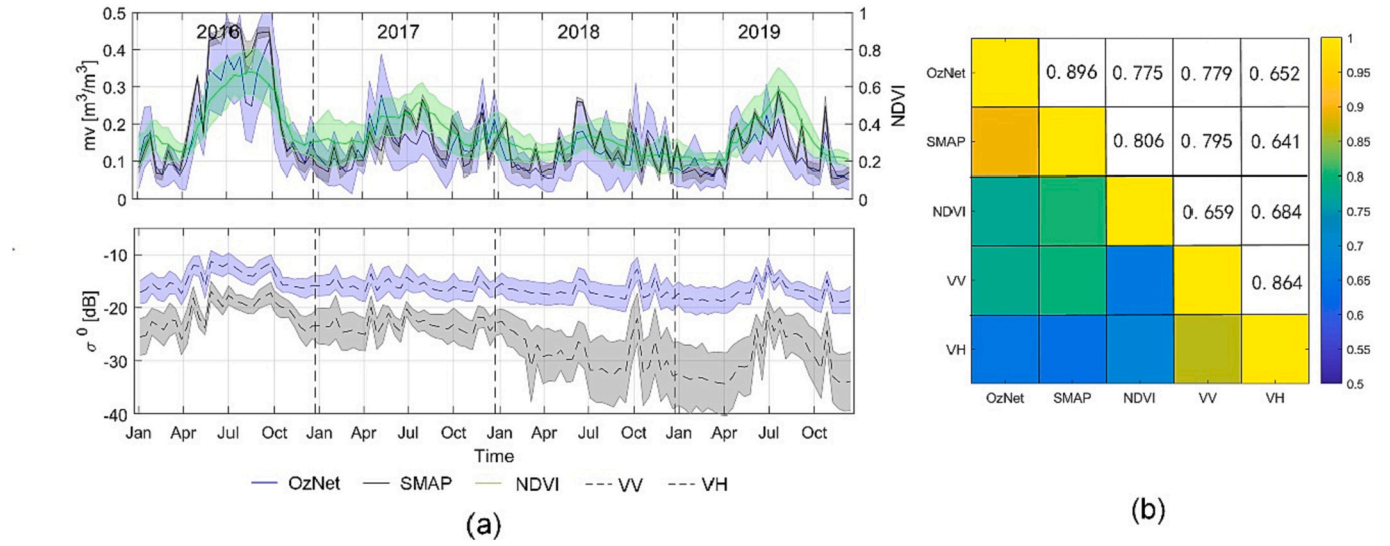

Fig. 3. Time series of OzNet, SMAP L3 soil moisture, NDVI and Sentinel-1 observations on the acquisition dates of Sentinel-1 (a) and their correlation heatmap (b). The solid line and envelope represent the average and standard deviation of the 34 OzNet sites.

250 m. This composite was then resampled and re-projected to the grid of the pre-processed Sentinel-1 data using the nearest neighbor method. The time series NDVI for all Sentinel-1 acquisition dates then were interpolated using a using a spline function. The time series SMAP L3 passive soil moisture over each station was extracted first based on the 36 km SMAP grids. Similarly, the soil moisture of each station on all Sentinel-1 acquisition dates were then interpolated with a spline function.

Fig. 3 shows the mean and standard deviation of OzNet, SMAP, NDVI, Sentinel-1 VV and VH across the 34 OzNet sites as well as the correlation heatmap. As expected, the OzNet soil moisture time series showed high correlation with Sentinel VV backscatter and SMAP soil moisture. The OzNet soil moisture also had a high correlation with the NDVI, being the main stress for the vegetation in this area. An abrupt increase of soil moisture can result in an abrupt increase of NDVI in dry seasons e.g., April to October 2018.

4. Results

4.1. The effect of vegetation constraint and assumption

The retrieval algorithm with time invariant vegetation (TFFF), time variant vegetation (FFFF) or temporal vegetation constraint (FTFF) was evaluated and compared across the 547 stations, first to show the effect of vegetation constraints (Fig. 4). The length of retrieval time window (N_t) ranged from 2 ($\leq$ 12 days) to 12 ($\leq$ 132 days) Sentinel-1 acquisitions with an interval of 2 ($\leq$ 24 days) acquisitions. The TFFF variant achieved the worst results in all cases of N_t with the ubRMSE being >0.11 m^3/m^3. The retrieval performance was improved after removing the assumption of time invariant vegetation (i.e., the FFFF variant) even for a short retrieval period of $\leq$12 days ($N_t = 2$). As N_t was increased, the ubRMSE of the FFFF variant slightly decreased at the expense of underestimating the standard deviation of the retrieved soil moisture. The algorithm using a temporal vegetation constraint (FTFF) achieved similar but slightly better results compared to the FFFF variant, with a larger decrease in retrieval standard deviation for a larger N_t.

The retrieved time series soil moisture, VWC and RMS heights of the 34 OzNet stations are depicted in Fig. 5, further illustrating the joint effect of N_t and the vegetation constraints. The VWC retrieved by the TFFF variant showed a smoother temporal evolution than that of the other two methods. The time invariant vegetation together with the sliding window processing (Fig. 1) was similar to a 1-dimension sliding

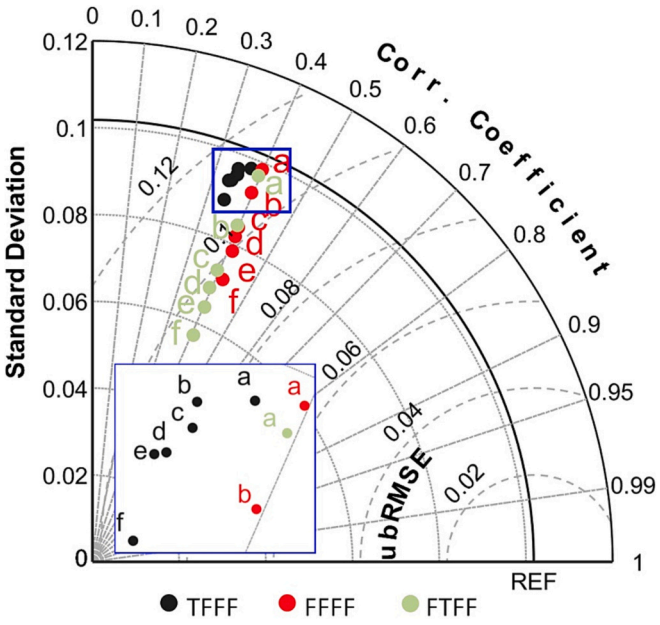

Fig. 4. Comparison of the retrieval algorithms with time invariant vegetation (TFFF), time variant vegetation (FFFF) and vegetation temporal constraint (FTFF); a-f refer to the results using a N_t varying from 2 to 12 with an interval of 2. The results for grass, crop and shrub and the results for all networks can be found in the supplementary document (Fig. S1 and S3), with similar patterns.

averaging filter with a size of N_t. The retrieved VWC maintained the four main vegetation peaks using a N_t of 4, while only the largest peak of Jul. – Oct. 2016 was captured with a N_t of 12. As a result, all the short-term vegetation variations were removed by the TFFF variant and the effect of such variations on backscattering was mis-interpreted as the change of roughness and/or soil moisture, being the main reason for the poor results and the relatively larger soil moisture variations (Fig. 4). In contrast, the time series VWC retrieved by the FFFF method can be decomposed into seasonal variations and abrupt changes. The later was observed to be accompanied by abrupt soil moisture changes (Fig. 3), which can be partly explained by the abrupt water supply from the soil moisture. Moreover, VWC and soil moisture can be overestimated concurrently to meet the real radar observations in the ill-posed

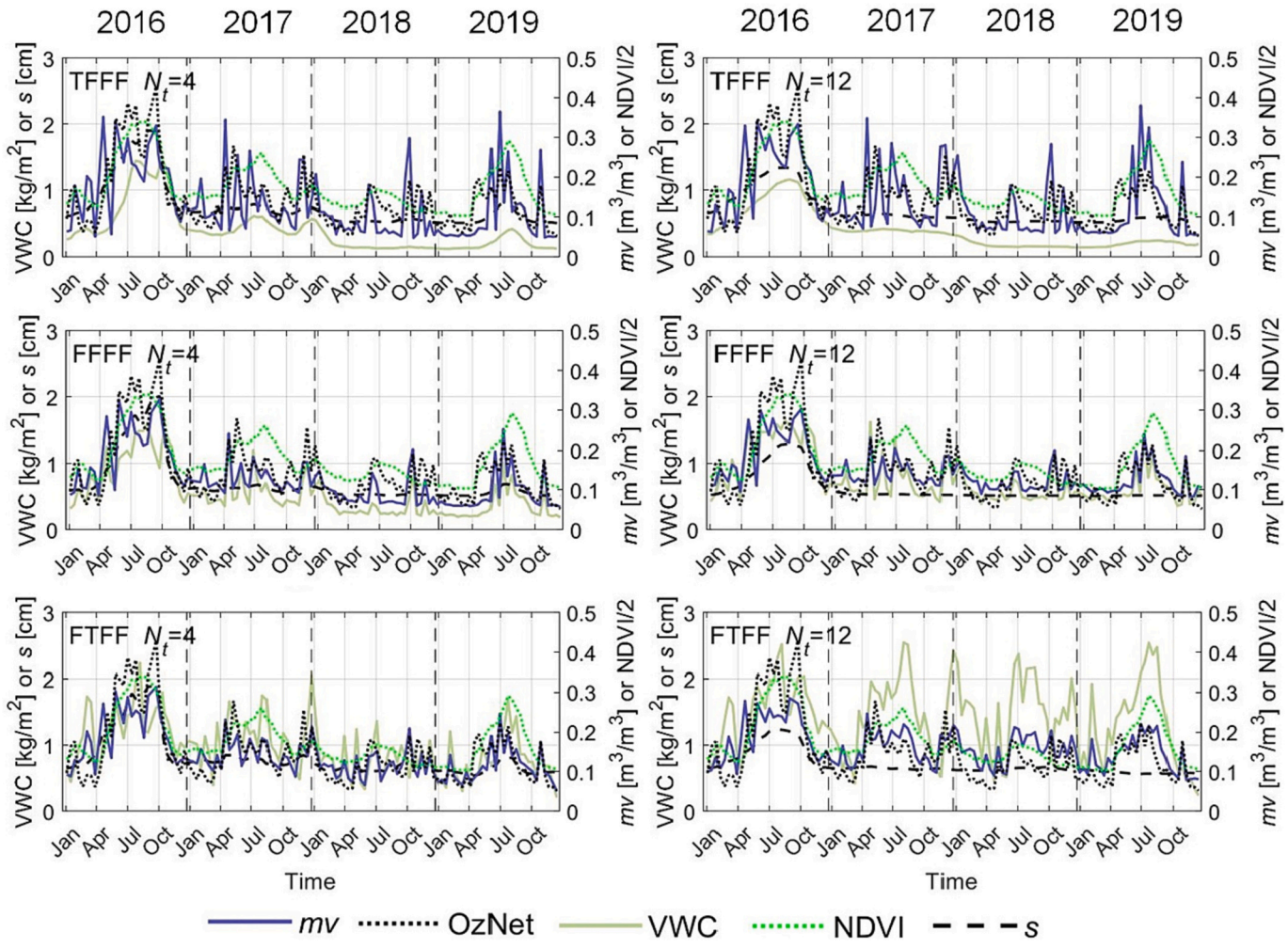

Fig. 5. Average soil moisture (*mv*), vegetation water content (VWC) and RMS height (*s*) of OzNet sites retrieved by the algorithm with time invariant vegetation (TFFF), time variant vegetation (FFFF,) and vegetation temporal constraint (FTFF) as well as the average NDVI and OzNet measurements. The left and right column are the results of using $N_t = 4$ and 12 respectively.

inversion of the FFFF variant, being another reason of the abrupt changes.

After applying the temporal vegetation constraint (i.e., the FTFF variant), the short-term temporal variation of retrieved VWC was further increased. In the inversion process of the FTFF variant, the cost function term representing VWC trends converged faster (Eq. 10) than the f_σ, and the VWC values were forced to meet the "correct" trend first. The range of VWC was observed to increase gradually before convergence, leading to a large inner-window variation. A larger N_t led to a larger variation in VWC which resulted in a larger inter-annual variation in soil moisture. The three vegetation temporal constraints thus act like "zoom in" to "zoom out" operations of soil moisture variation, with their effects being enhanced using a larger N_t.

The retrieved roughness showed limited temporal variation (Fig. 5) except the peak in the middle of 2016, generally ranging from 0.5 to 0.8 cm. Notably, the retrieved roughness values were effective values and can therefore be substantially different from the ground measurements, as a result of the uncertainty of the scattering models (Baghdadi and Zribi, 2011; Lievens et al., 2011; Zhu et al., 2016). The retrieved RMS heights followed the trend of the VWC in the results of the TFFF and FFFF method, playing a similar role of VWC in the optimization process. A more comprehensive analysis on the 457 stations is provided in Fig. S4. This confirmed that assuming a time invariant roughness for a long retrieval period is also questionable, not only for the potential changes in ground roughness, but also for the requirement of varying effective roughness values in the optimization process.

4.2. The effect of soil moisture constraint and assumption

The retrieval algorithms with soil moisture bounds (FFTF), soil moisture temporal constraint (FFFT) and both soil moisture constraints (FFTT) were evaluated across the 547 stations, with the FFFF being included as the benchmark (Fig. 6). The comparison of the FFFF and FFTF methods showed that the use of reliable soil moisture bounds can substantially improve the retrieval performance. The average ubRMSE decreased from 0.103 to 0.087 m^3/m^3, while the average *R* increased from 0.40 to 0.59. In contrast, single use of the temporal soil moisture constraint led to deterioration in accuracy, with an average decrease of 0.06 in R. The joint use of the two soil moisture constraints (FFTT) achieved the best results, with an average ubRMSE and R of 0.086 m^3/m^3 and 0.61 respectively. While the difference in ubRMSE and R was marginal for different N_t, the standard deviation of retrieved soil moisture gradually decreased as N_t increased for all algorithms, being consistent with the results of Fig. 4. The FFTT method showed the smallest sensitivity to N_t, suggesting a relatively stable performance for a longer retrieval window.

Fig. 7 shows the average soil moisture, VWC and RMS heights of the 34 OzNet stations retrieved by three algorithms using different soil moisture constraints. The FFFT failed to capture the general trend of soil moisture and substantially overestimated the short-term (2–4 weeks)

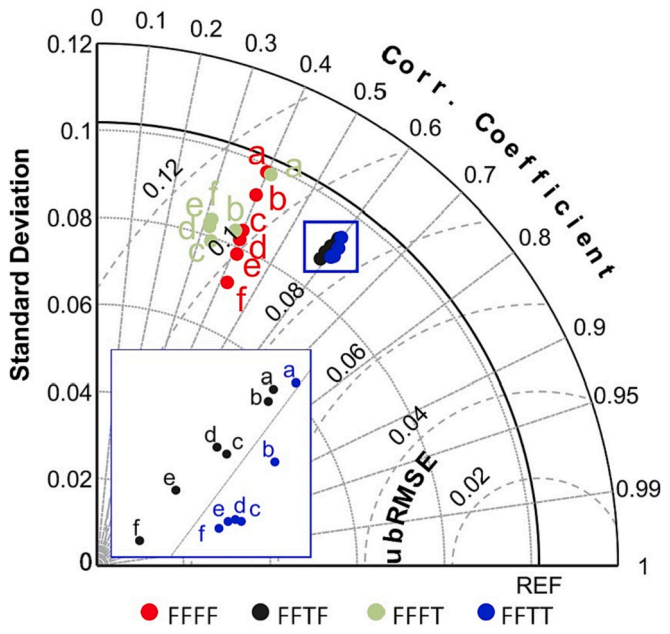

Fig. 6. Same as Fig. 4 but for soil moisture bounds (FFTF), soil moisture temporal constraint (FFFT) or both soil moisture bound and temporal constraints (FFTT). The results for grass, crop and shrub can be found in the supplementary document (Fig. S3), with similar patterns.

temporal variations. Specifically, the retrieved soil moisture within each retrieval window achieved a similar range of 0.1–0.3 m^3/m^3 for the case of $N_t = 4$, which extended to 0.1–0.5 m^3/m^3 when $N_t = 12$. This suggests that the effect of the soil moisture temporal constraint on retrieval is similar to that of the vegetation temporal constraint, substantially increasing the short-term temporal variation of soil moisture and thus VWC. In contrast, the FFTF method well captured the general trend and accurately reflected the soil moisture ranges of various periods. For example, the FFTF had smaller underestimation of the high soil moisture observed in the Australian winter of 2016 than retrievals without the soil moisture bounds. However, the retrieved soil moisture of FFTF showed smaller short-term variations compared to that of the FFFF method (Fig. 5) and the OzNet observations (Fig. 3). Therefore, the time series soil moisture retrieved by the FFTT seemed to be a compromise of the FFTF and FFFT methods. In view of a signal, the time series retrieved by the FFFT and FFTF methods were like the high and low frequency components of the FFTT time series respectively. Moreover, the amplitude of the high frequency components could be amplified using a longer retrieval window, while the low frequency components could also be enhanced by depressing the high frequency components with a longer retrieval window.

4.3. The joint effect of constraints and ensemble

The bias, R, RMSE and ubRMSE of all sites were calculated for the single retrievals and ensemble retrievals (Fig. 8), with the single retrievals using the full time series of Sentinel-1 (i.e., $N_e = 1$ in Fig. 1). For simplicity, only the results of $N_t = 4$ are presented as it is the default value for various time series methods (Al-Khaldi et al., 2019; Balenzano et al., 2021; He et al., 2017; Ouellette et al., 2017; Zhu et al., 2022). The 4 algorithms with soil moisture bounds (i.e., FFTF, FFTT, FTTF and FTTT) achieved a near-zero median bias (<0.007 m^3/m^3) on both single and ensemble retrieval modes, being significantly lower than that of the other methods without soil moisture bounds (0.026–0.042 m^3/m^3). Apart from a smaller bias, the use of soil moisture bounds resulted in significant higher R, lower RMSE and ubRMSE. The average improvement in R, RMSE and ubRMSE from using soil moisture bounds is 0.277, 0.033 m^3/m^3 and 0.027 m^3/m^3 respectively for the single retrievals, which is 0.286, 0.029 m^3/m^3 and 0.023 m^3/m^3 for the ensemble retrievals. This further suggests that the soil moisture bounds are the most useful constraint.

Among the four algorithms using the soil moisture bounds, the FFTT method achieved the best results in median RMSE and R (0.072 m^3/m^3 and 0.643), followed by the FTTT (RMSE: 0.072 m^3/m^3, R: 0.641), FTTF (RMSE: 0.073 m^3/m^3, R: 0.609) and FFTF (RMSE: 0.074 m^3/m^3, R:0.603). This suggests that extra use of the soil moisture and/or vegetation temporal constraint can lead to better but insignificant results. However, the joint use of two temporal constraints without the soil moisture bounds (i.e., the FTFT method) led to the worst results among the algorithms that used multiple constraints. This can be explained by that either the soil moisture or the vegetation temporal constraint can increase the short-term soil moisture variations (Fig. 5 and Fig. 7) which was further enhanced by the joint use of two temporal constraints. The ensemble retrievals outperformed the single retrievals on all algorithm variants in R, RMSE and ubRMSE, with the average improvement in median values being ~0.04, ~ 0.005 m^3/m^3 and ~ 0.005 m^3/m^3, respectively. As expected, the difference between single and ensemble retrievals in bias was negligible (< 0.001) as the ensemble average of multiple sub-retrievals retain the system bias. The difference in RMSE was only significant for 4 algorithm (TFFF, FFFF, FTFF and FTFT) and all these methods showed relatively higher RMSEs than the others. Similarly, the difference in ubRMSE was insignificant for the two most powerful variants (FFTT and FTTT), suggesting that weaker algorithms can probably benefit more from ensemble retrievals. Same to the ensemble retrievals, the single retrieval using the FFTT method achieved the best results followed by the FTTT, FTTF and FFTF method, suggesting that the use of ensemble retrieval cannot change the relative performance of the 9 variants.

4.4. Evaluation over the SMAPEx-5 focus areas

A further investigation was made on the SMAPEx-5 data set (Fig. 2). Similar to the results on the 547 stations, the ensemble retrievals achieved better results than the corresponding single retrievals on all methods except the FFTF method (Fig. 9). The average improvement of using the ensemble concept was ~0.007 m^3/m^3 in ubRMSE and ~ 0.05 in R. These improvements were mainly from the reduced random uncertainty contained in data, scattering models and assumptions, with the pattern of ground measured versus retrieved being less scattered (Fig. 10). This however is not always positive, probably overestimating the low values and underestimating the high values. Consequently, the improvement in R can be larger than that in RMSE as the bias can be increased, being consistent with Fig. 8. Different from the results on the global dataset, the use of soil moisture bounds and the two vegetation constraints contributed little, and even negatively to the SMAPEx-5 scenario. For example, the TFFF method showed a competitive performance to the FFTT method. The potential reasons include: 1) the range of soil moisture in SMAPEx-5 was close to the global soil moisture range of 0.03–0.47 m^3/m^3 and thus the use of SMAP based soil moisture bounds could not add any useful constraint and 2) the VWC during the SMAPEx-5 was nearly time-invariant (Ye et al., 2020) and thus the assumption of time-invariant VWC can be more reliable.

Fig. 10 shows the soil moisture maps for the SMAPEx-5 focus area on Sep. 14, 2015. The retrieved soil moisture maps of the 9 algorithms had similar spatial patterns, which generally matched the pattern of ground measurements. The bare soil had smaller soil moisture values, followed by grass land and the areas with crops (mainly wheat). Consistent with the evaluation results on the global data set (Fig. 4 and 6), the soil moisture maps retrieved by different algorithms showed a similar average value but a large difference in standard deviation. The ensemble retrievals showed smaller spatial variations due to the ensemble average of multiple retrievals, in line with the evaluation on the SMAPEx-5 data set (Fig. 9).

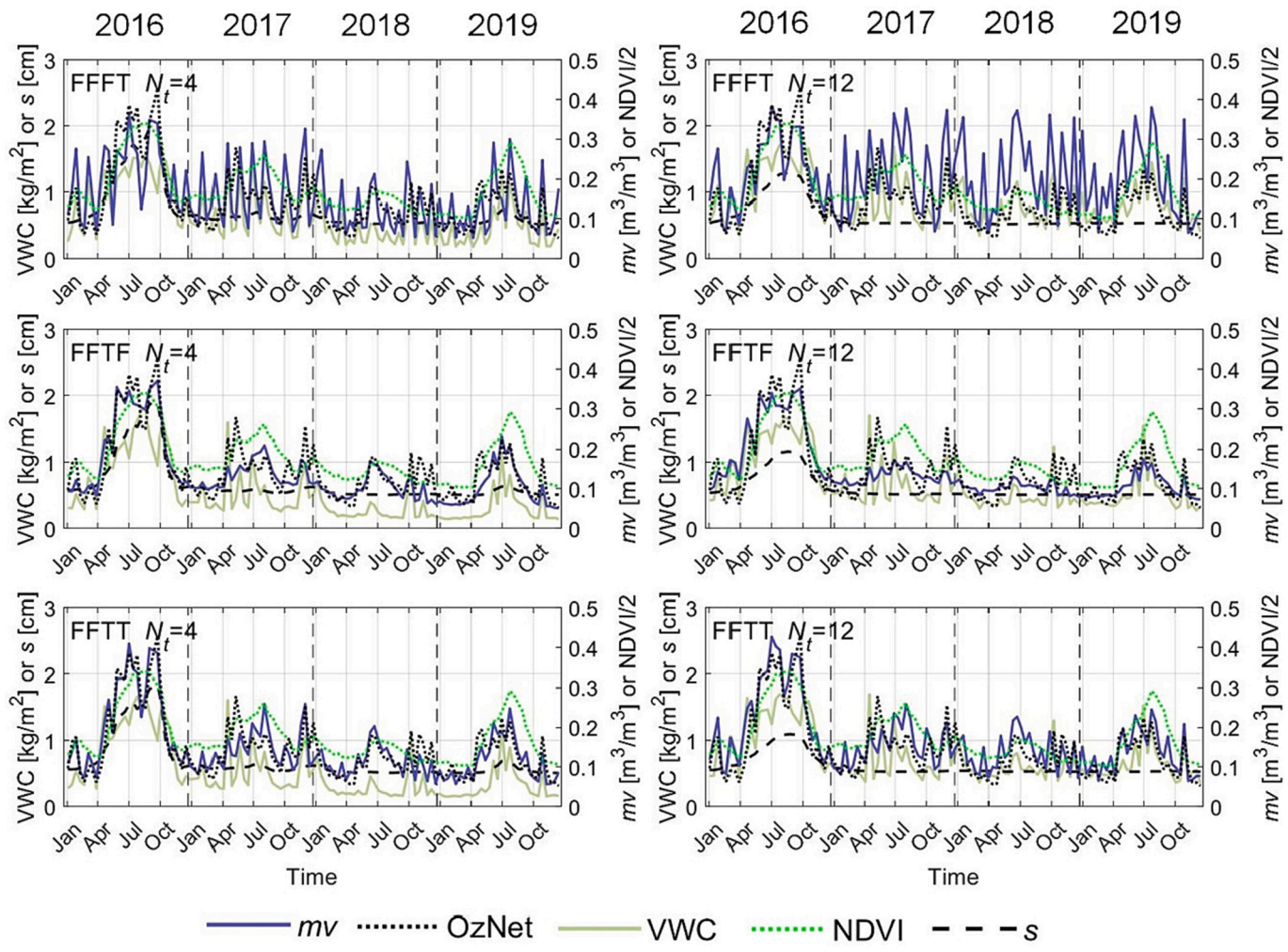

Fig. 7. Same as for Fig. 5 but for the algorithm with soil moisture bounds (FFTF), soil moisture temporal constraint (FFFT) and both soil moisture bound and temporal constraints (FFTT).

5. Discussion

The effect of four temporal constraints and the ensemble skill on time series soil moisture retrieval was investigated, providing some straightforward suggestions on how to constrain scattering-model based time series retrievals. The widely used assumption of time-invariant vegetation contributed negatively to the retrieval accuracy in the global validation, even for a short retrieval period of $\leq$12 days ($N_t = 2$ in Fig. 4 and Fig. S3). However, it still improved the retrieval accuracy for specific areas and periods, such as the SMAPEx-5 scenario (Fig. 9). The negative effect of the time-invariant vegetation can be partly ascribed to the vegetation changes, with a longer retrieval window meaning poorer results (Palmisano et al., 2020). Moreover, the assumption of time-invariant roughness and vegetation forced a smooth evolution of VWC and roughness in the retrieval process (Fig. 6), with the short-term variation of radar observations and scattering model uncertainties all being ascribed to the variation of soil moisture. The retrieved time series VWC may accurately reflect the variation of real vegetation but this is not necessary to result in better soil moisture retrieval, because effective values can be more favorable for inversing a moderate scattering model. Similarly, many studies found that the direct use of ground measured roughness in soil moisture retrieval is questionable and effective values based on scattering models can be more useful (Baghdadi and Zribi, 2011; Lievens et al., 2011; Zhu et al., 2016). This suggests that an over-constrained inversion does not necessarily result in good results when an imperfect scattering model was used.

The proposed two temporal constraints are qualitative descriptions of the temporal evolution of vegetation and soil moisture, being relatively weaker constraints compared to the assumptions of time-invariant vegetation. Since these relationships are easier to be achieved and more reliable than empirical modelling of temporal vegetation or soil moisture dynamics (Kim et al., 2017; Wagner et al., 1999a), they were expected to provide safer prior knowledge for improved soil moisture retrievals. However, single use of either constraint was found to contribute negatively to the retrieval accuracy in the global validation (Fig. 4 and 6), introducing substantial short-term variations in soil moisture. A conflicting conclusion was made in two previous studies where soil moisture after a rainfall event was forced to decrease monotonously (Zhu et al., 2019a, 2019b). The temporal constraints contributed positively if they were used together with soil moisture bounds (Fig. 8 and Fig. 10). The two previous studies inherently used the soil moisture bounds, because the real soil moisture bounds were close to those of the LUTs (Zhu et al., 2019a, 2019b), and thus the temporal constraint of soil moisture contributed positively. Moreover, time series multi-angular and multi-frequency data was used in the two previous studies with larger uncertainties in data and scattering models, being more challenging than the time series retrieval from a single data source. Consequently, a further investigation using a long time series of multi-angular and multi-frequency data (e.g., the joint time series of Sentinel-1 and SAOCOM-1) can be valuable for the use of these temporal constraints.

The soil moisture range was confirmed to be critical for a successful

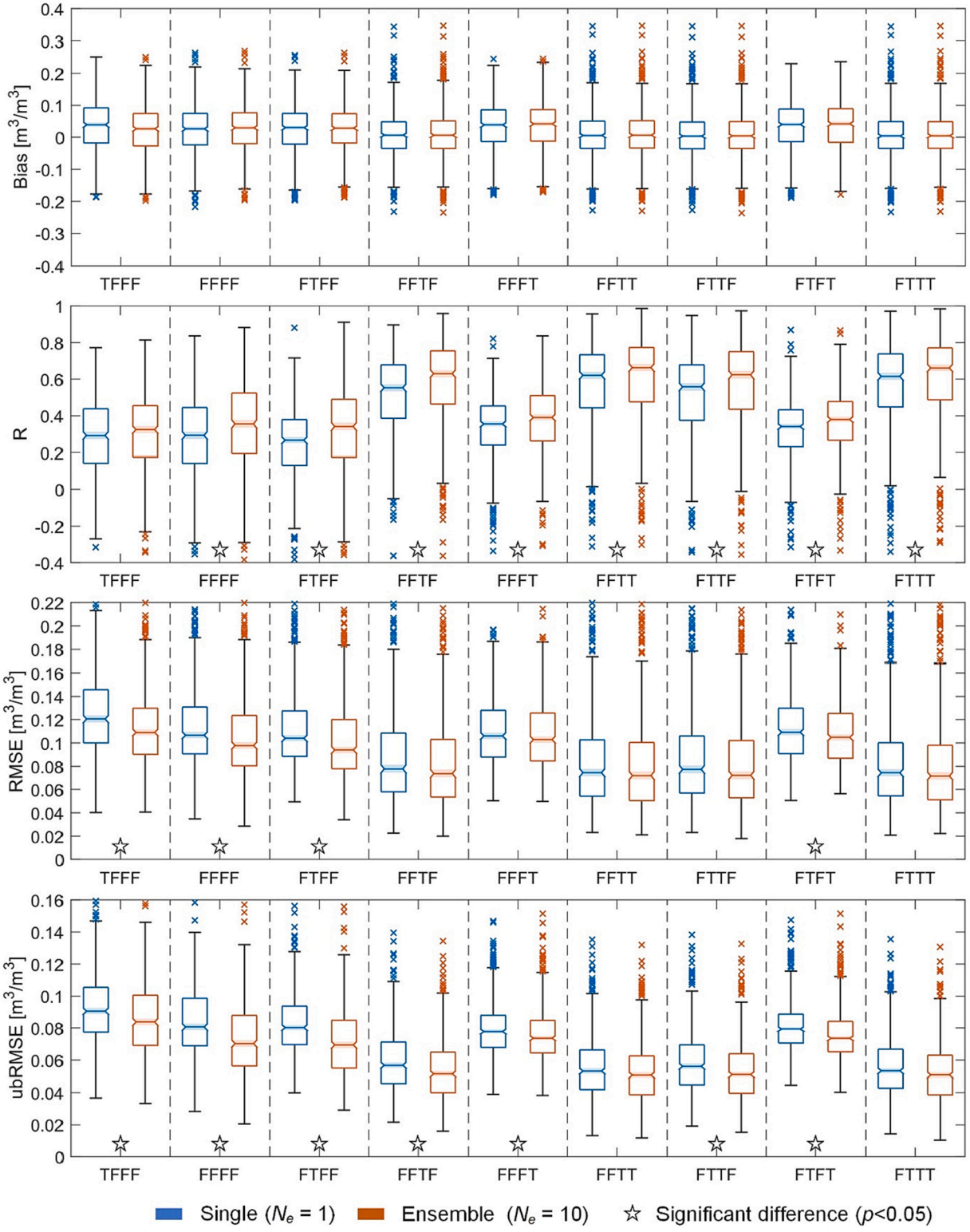

Fig. 8. Performance of the 9 algorithms using the single ($N_e = 1$ in Fig. 1 with full VV/VH time series) and ensemble retrieval mode ($N_e = 10$) on the 547 stations, with the top to bottom panel being bias, R, RMSE and ubRMSE respectively. The default $N_t = 4$ was used.

retrieval, being consistent with the short-term change detection algorithms (He et al., 2017; Ouellette et al., 2017). In this study, the global soil moisture range used is that of the LUTs (0.03 to 0.47 m^3/m^3), considering the typical calibration error of ground measurements (Smith et al., 2012) and the fact that the scattering model uncertainty (e.g., 2 dB) can be much larger than the sensitivity of the radar signal to high soil moisture values. This range generally covers the natural soil conditions observed from very dry to wet, with only a limited number of observations (150 out of 68,468; ~0.22%) from the 547 stations exceeding 0.47 m^3/m^3 for the study period. The range of time series coarse soil moisture products of SMAP (36 km) was used for a more reliable estimation of a specific retrieval window. Other model-based

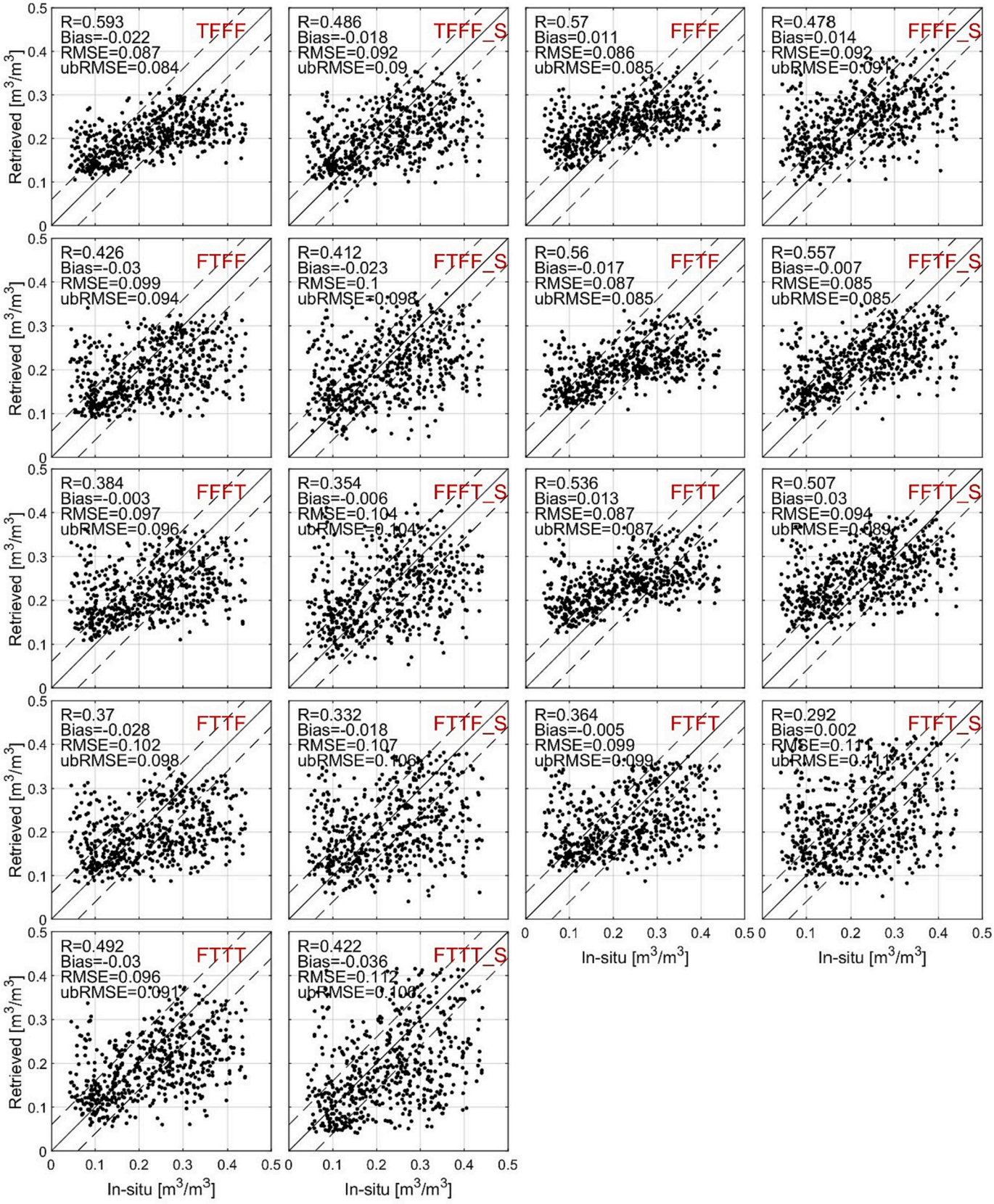

Fig. 9. Performance of ensemble (first and third column) and single (second and fourth column) retrievals on the SMAPEx-5 data set using a $N_t = 4$ retrieved according to the 9 retrieval algorithms (see Table 1).

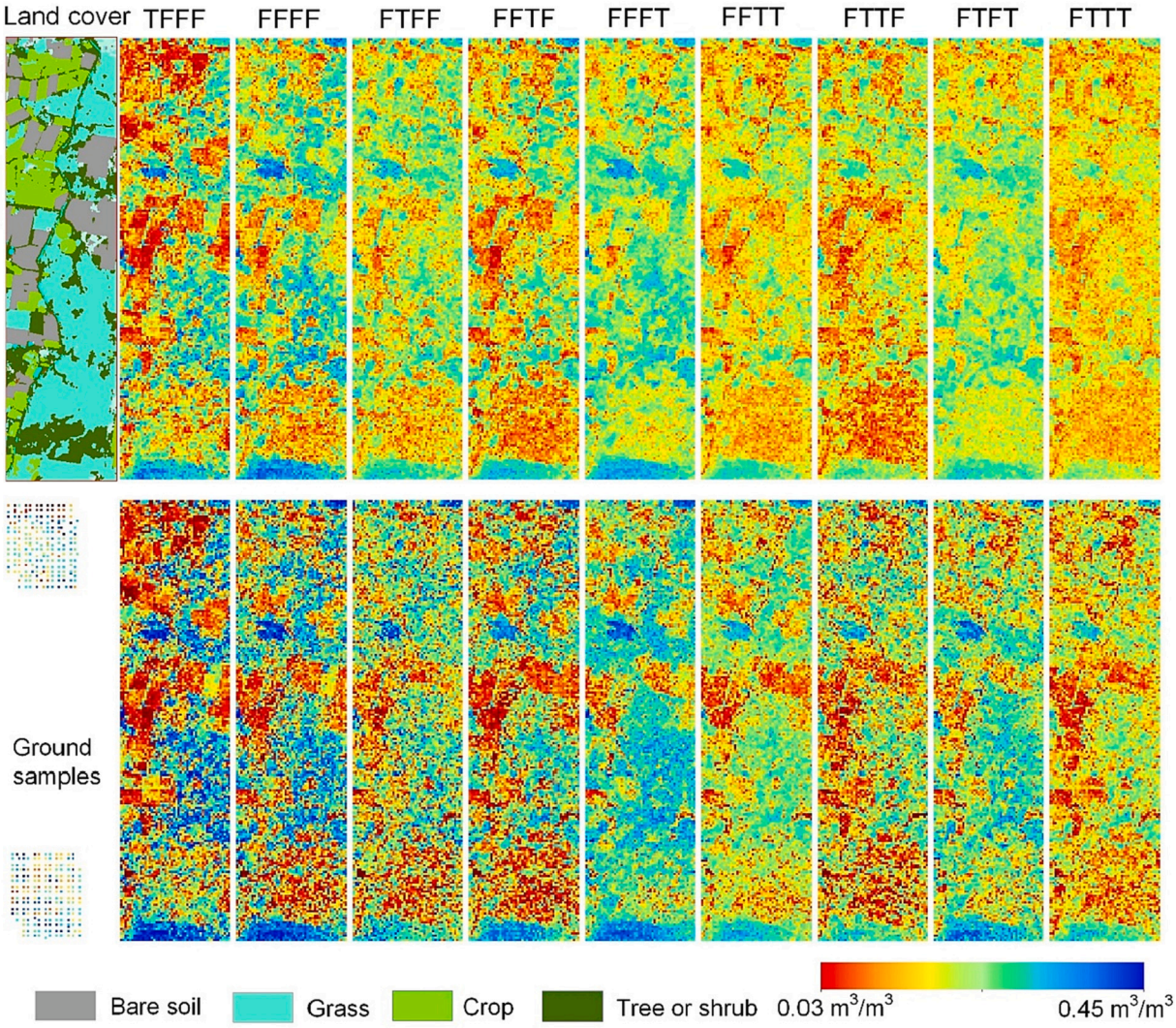

Fig. 10. The soil moisture maps of Sep. 14, 2015 retrieved by the 9 algorithms (see Table 1) with ensemble (top panel) and without ensemble (bottom panel). The landcover was from Ye et al. (2020).

soil moisture products (e.g., the fifth generation of ECMWF atmospheric reanalyzes, ERA-5) can be promising alternatives, with the advantage of providing long-term continuity; refer to the Fig. S7-S9 for a comparison of using ERA5-Land and SMAP L3 in soil moisture retrieval. Nevertheless, use of such coarse soil moisture products could not fully retain the large spatial and temporal variations of soil moisture at a grid size of 100 m. Consequently, the retrieved soil moisture showed a smaller standard deviation both spatially (Fig. 10) and temporally (Fig. 6). Fortunately, extra use of the soil moisture temporal constraint could partly recover the temporal variation (Fig. 4 and 6).

The effectiveness of the ensemble retrieval concept was demonstrated in Zhu et al. (2020) using a synthetic data set with various incidence angles, polarizations, frequencies and uncertainty sources. Its effectiveness for a real scenario of a long time series data was first confirmed in this study, with the improvement in RMSE being up to 0.013 m^3/m^3. While the improvement on 3 of the 9 algorithms was insignificant and the absolute improvement is limited, the ensemble skill has no interaction with the 4 constraints in the inversion process and thus can be compatible with any combination of the 4 constraints. However, the ensemble retrievals were prone to underestimate the range and spatial variation of soil moisture by removing the largest and/or smallest estimations in the ensemble average (Fig. 9 and Fig. 10). The use of soil moisture bounds and the assumption of time-invariant vegetation also tended to result in a smoother temporal evolution and smaller spatial variation. The joint use of these constraints and the ensemble can further reduce the variation, e.g. the results of the FFTF method in Fig. 9.

The length of retrieval window (N_t) is a key parameter of the presented multi-temporal inversion scheme as well as existing time series methods. Different from the simple conclusion that a larger N_t means larger retrieval error (Palmisano et al., 2020), the effect of N_t on soil moisture retrieval varied when different constraints were applied, as summarized in Table 3. The retrievals without constraint achieved better accuracy statistics from an increased N_t, which however led to a

Table 3
The effect of an increased N_t on the performance of algorithms using various constraints.

Constraint	Accuracy	Variation of the retrieved soil moisture
No constraint	Increase	Decrease
Soil moisture bounds	Decrease	Decrease
Time-invariant vegetation	Unclear trend	Unclear trend
Vegetation temporal constraint	Increase	Decrease
Soil moisture temporal constraint	Decrease	Increase

smaller and underestimated soil moisture variation. A similar behavior was observed for the retrievals with vegetation temporal constraints. Accordingly, the algorithms with a single constraint cannot benefit from an increased N_t. However, the joint use of two soil moisture constraints resulted in negligible difference in accuracy statistics and retained the variation of retrieved soil moisture for a N_t up to 12, suggesting that the FFTT and FTTT method can be used in a much longer retrieval window beyond the current experience of 1–4 weeks.

Apart from the perspectives on how to constrain the inversion process of time series retrieval, this study provided a near-operational time series scheme for soil moisture retrieval from Sentinel-1 IW GRD data. Some of the 9 algorithm variants achieved a competitive median RMSE and ubRMSE of ~0.072 and ~ 0.051 m^3/m^3 at a grid size of 100 m, with the performance of the best variant (FFTT) on the 547 stations being provided in the supplementary document (Fig. S7). The accuracy statistics can be further improved when retrieval or evaluated at a coarser grid of e.g., 1 km. Although the parametrization and calibration of the scattering models still required ground measurements, the LUTs initially built for the SMAPEx-5 were successfully applied for the entire period of 2016–2019 and 547 worldwide stations without further calibration or modification. However, the large performance discrepancy among the 547 stations (Fig. 8 and S7) and 17 networks (Fig. S6), suggested that the LUTs based on the SMAPEx-5 cannot fully represent the surface conditions of all networks. The current LUTs only covered grass and crop types that were dominated by a single layer of vertical structure, with further extensions for other types being possible (Kim et al., 2014). The VWC was limited to <4 kg/m^2, considering the limited soil contributions at larger values (Zhu et al., 2019a). However, this boundary and the validity of C-band for dense vegetated areas are still questionable, requiring a location mask based on landcover maps and thresholds for volume scattering dominated areas (Balenzano et al., 2021).

6. Conclusion

The effect of four temporal constraints and the ensemble skill on time series soil moisture retrieval was investigated using the soil moisture measurements of 547 stations from 17 networks along with intensive ground measurements from the SMAPEx-5. While the effect of these temporal retrieval skills varied across stations and networks, and was also related to the robustness of the scattering models, four empirical suggestions for global applications are made: 1) assuming time-invariant vegetation contributed negatively in the global validation as a result of potential vegetation changes and over-constrained inversion of moderate scattering models; 2) reliable information of soil moisture bounds is critical for successful retrieval with the risk of underestimating the soil moisture variation; 3) the two temporal constraints of vegetation and soil moisture must be used together with the soil moisture bounds to maintain the variation of soil moisture; and 4) the use of an ensemble can benefit the soil moisture retrieval by partly removing uncertainties at the expense of underestimating the soil moisture variation. The proposed time series inversion scheme with these inversion skills achieved a competitive retrieval accuracy (median RMSE: ~0.072 m^3/m^3, median R: 0.64) at a high resolution of 100 m, with its generalization capability confirmed for a long period of 4 years.

CRediT authorship contribution statement

Liujun Zhu: Conceptualization, Methodology, Writing – original draft. **Shanshui Yuan:** Writing – original draft, Writing – review & editing. **Yi Liu:** Writing – review & editing. **Cheng Chen:** Writing – review & editing. **Jeffrey P. Walker:** Writing – review & editing.

Declaration of Competing Interest

The authors declare that they have no known competing financial interests or personal relationships that could have appeared to influence the work reported in this paper.

Data availability

Data will be made available on request.

Acknowledgments

This work was supported by the National Natural Science Foundation of China (42101374 and 52121006), the Fundamental Research Funds for the Central Universities (B220201009) and the Basic Research Project of Jiangsu Province (BK20210377 and BK20210368). The SMAPEx-5 field campaign was supported by an Australian Research Council Discovery Project (DP140100572). The authors express sincere thanks to the data providers and the International Soil Moisture Network for the network data listed in Table 1. Finally, the authors are grateful to the Reviewers for their valuable comments which helped to improve the quality of this paper.

Appendix A. Supplementary data

Supplementary data to this article can be found online at https://doi.org/10.1016/j.rse.2023.113466.

References

Al-Khaldi, M.M., Johnson, J.T., O'Brien, A.J., Balenzano, A., Mattia, F., 2019. Time-series retrieval of soil moisture using CYGNSS. IEEE Trans. Geosci. Remote Sens. 57, 4322–4331.
Attema, E., Ulaby, F.T., 1978. Vegetation modeled as a water cloud. Radio Sci. 13, 357–364.
Baghdadi, N., Holah, N., Zribi, M., 2006. Soil moisture estimation using multi-incidence and multi-polarization ASAR data. Int. J. Remote Sens. 27, 1907–1920.
Baghdadi, N., Zribi, M., 2011. Evaluation of radar backscatter models IEM, OH and Dubois using experimental observations. Int. J. Remote Sens. 27, 3831–3852.
Balenzano, A., Mattia, F., Satalino, G., Davidson, M.W., 2011. Dense temporal series of C- and L-band SAR data for soil moisture retrieval over agricultural crops. IEEE J. Sel. Top. Appl. Earth Obs. Remote Sens. 4, 439–450.
Balenzano, A., Mattia, F., Satalino, G., Lovergine, F.P., Palmisano, D., Peng, J., Marzahn, P., Wegmüller, U., Cartus, O., Dąbrowska-Zielińska, K., 2021. Sentinel-1 soil moisture at 1 km resolution: a validation study. Remote Sens. Environ. 263, 112554.
Bauer-Marschallinger, B., Freeman, V., Cao, S., Paulik, C., Schaufler, S., Stachl, T., Modanesi, S., Massari, C., Ciabatta, L., Brocca, L., 2018. Toward global soil moisture monitoring with Sentinel-1: harnessing assets and overcoming obstacles. IEEE Trans. Geosci. Remote Sens. 57, 520–539.
Bell, J.E., Palecki, M.A., Baker, C.B., Collins, W.G., Lawrimore, J.H., Leeper, R.D., Hall, M.E., Kochendorfer, J., Meyers, T.P., Wilson, T., 2013. US climate reference network soil moisture and temperature observations. J. Hydrometeorol. 14, 977–988.
Bindlish, R., Barros, A.P., 2000. Multifrequency soil moisture inversion from SAR measurements with the use of IEM. Remote Sens. Environ. 71, 67–88.
Blöschl, G., Blaschke, A., Broer, M., Bucher, C., Carr, G., Chen, X., Eder, A., Exner-Kittridge, M., Farnleitner, A., Flores-Orozco, A., 2016. The hydrological open air laboratory (HOAL) in petzenkirchen: a hypothesis-driven observatory. Hydrol. Earth Syst. Sci. 20, 227–255.
Bousbih, S., Zribi, M., El Hajj, M., Baghdadi, N., Lili-Chabaane, Z., Gao, Q., Fanise, P., 2018. Soil moisture and irrigation mapping in a semi-arid region, based on the synergetic use of Sentinel-1 and Sentinel-2 data. Remote Sens. 10, 1953.
Buchhorn, M., Lesiv, M., Tsendbazar, N.-E., Herold, M., Bertels, L., Smets, B., 2020. Copernicus global land cover layers—collection 2. Remote Sens. 12, 1044.
Callens, M., Verhoest, N.E., Davidson, M.W., 2006. Parameterization of tillage-induced single-scale soil roughness from 4-m profiles. IEEE Trans. Geosci. Remote Sens. 44, 878–888.
Calvet, J.-C., Fritz, N., Berne, C., Piguet, B., Maurel, W., Meurey, C., 2016. Deriving pedotransfer functions for soil quartz fraction in southern France from reverse modeling. Soil 2, 615–629.
Chen, K.-S., Wu, T.-D., Tsang, L., Li, Q., Shi, J., Fung, A.K., 2003. Emission of rough surfaces calculated by the integral equation method with comparison to three-dimensional moment method simulations. IEEE Trans. Geosci. Remote Sens. 41, 90–101.
Cook, D.R., 2016. Soil temperature and moisture profile (STAMP) system handbook.. In: DOE Office of Science Atmospheric Radiation Measurement (ARM) Program.
Cui, C., Xu, J., Zeng, J., Chen, K.-S., Bai, X., Lu, H., Chen, Q., Zhao, T., 2017. Soil moisture mapping from satellites: an intercomparison of SMAP, SMOS, FY3B, AMSR2, and ESA CCI over two dense network regions at different spatial scales. Remote Sens. 10, 33.

Deb, K., 2014. Multi-objective optimization. In: Search methodologies. Springer, pp. 403–449.
Demargne, J., Wu, L., Regonda, S.K., Brown, J.D., Lee, H., He, M., Seo, D.-J., Hartman, R., Herr, H.D., Fresch, M., 2014. The science of NOAA's operational hydrologic ensemble forecast service. Bull. Am. Meteorol. Soc. 95, 79–98.
Dorigo, W., Himmelbauer, I., Aberer, D., Schremmer, L., Petrakovic, I., Zappa, L., Preimesberger, W., Xaver, A., Annor, F., Ardö, J., 2021. The international soil moisture network: serving earth system science for over a decade. Hydrol. Earth Syst. Sci. 25, 5749–5804.
Dubois, P.C., Van Zyl, J., Engman, T., 1995. Measuring soil moisture with imaging radars. IEEE Trans. Geosci. Remote Sens. 33, 915–926.
El Hajj, M., Baghdadi, N., Zribi, M., Belaud, G., Cheviron, B., Courault, D., Charron, F., 2016. Soil moisture retrieval over irrigated grassland using X-band SAR data. Remote Sens. Environ. 176, 202–218.
Fan, D., Zhao, T., Jiang, X., Xue, H., Moukomla, S., Kuntiyawichai, K., Shi, J., 2021. Soil moisture retrieval from Sentinel-1 time-series data over croplands of northeastern Thailand. IEEE Geosci. Remote Sens. Lett. 19, 4011105.
Fung, A.K., 1994. Microwave scattering and emission models and their applications. Artech House.
Galle, S., Grippa, M., Peugeot, C., Moussa, I.B., Cappelaere, B., Demarty, J., Mougin, E., Panthou, G., Adjomayi, P., Agbossou, E., 2018. AMMA-CATCH, a critical zone observatory in West Africa monitoring a region in transition. Vadose Zone J. 17, 1–24.
González-Zamora, Á., Sánchez, N., Pablos, M., Martínez-Fernández, J., 2019. CCI soil moisture assessment with SMOS soil moisture and in situ data under different environmental conditions and spatial scales in Spain. Remote Sens. Environ. 225, 469–482.
Gu, W., Tsang, L., Colliander, A., Yueh, S.H., 2021. Wave propagation in vegetation field using a hybrid method. IEEE Trans. Antennas Propag. 69, 6752–6761.
He, L., Qin, Q., Panciera, R., Tanase, M., Walker, J.P., Hong, Y., 2017. An extension of the alpha approximation method for soil moisture estimation using time-series SAR data over bare soil surfaces. IEEE Geosci. Remote Sens. Lett. 14, 1328–1332.
Huang, S., Tsang, L., 2012. Electromagnetic scattering of randomly rough soil surfaces based on numerical solutions of Maxwell equations in three-dimensional simulations using a hybrid UV/PBTG/SMCG method. IEEE Trans. Geosci. Remote Sens. 50, 4025–4035.
Jensen, K.H., Refsgaard, J.C., 2018. HOBE: the danish hydrological observatory. Vadose Zone J. 17, 1–24.
Joseph, A.T., van der Velde, R., O'Neill, P.E., Lang, R.H., Gish, T., 2008. Soil moisture retrieval during a corn growth cycle using L-band (1.6 GHz) radar observations. IEEE Trans. Geosci. Remote Sens. 46, 2365–2374.
Kellogg, K., Hoffman, P., Standley, S., Shaffer, S., Rosen, P., Edelstein, W., Dunn, C., Baker, C., Barela, P., Shen, Y., 2020. NASA-ISRO synthetic aperture radar (NISAR) mission. In: 2020 IEEE Aerospace Conference. IEEE, pp. 1–21.
Kim, S.-B., Moghaddam, M., Tsang, L., Burgin, M., Xu, X., Njoku, E.G., 2014. Models of L-band radar backscattering coefficients over global terrain for soil moisture retrieval. IEEE Trans. Geosci. Remote Sens. 52, 1381–1396.
Kim, S.-B., Tsang, L., Johnson, J.T., Huang, S., Van Zyl, J.J., Njoku, E.G., 2012. Soil moisture retrieval using time-series radar observations over bare surfaces. IEEE Trans. Geosci. Remote Sens. 50, 1853–1863.
Kim, S.-B., van Zyl, J.J., Johnson, J.T., Moghaddam, M., Tsang, L., Colliander, A., Dunbar, R.S., Jackson, T.J., Jaruwatanadilok, S., West, R., 2017. Surface soil moisture retrieval using the L-band synthetic aperture radar onboard the soil moisture active-passive satellite and evaluation at Core validation sites. IEEE Trans. Geosci. Remote Sens. 55, 1897–1914.
Kim, Y., Van Zyl, J.J., 2009. A time-series approach to estimate soil moisture using polarimetric radar data. IEEE Trans. Geosci. Remote Sens. 47, 2519–2527.
Kornelsen, K.C., Coulibaly, P., 2013. Advances in soil moisture retrieval from synthetic aperture radar and hydrological applications. J. Hydrol. 476, 460–489.
Lang, R.H., Sighu, J.S., 1983. Electromagnetic backscattering from a layer of vegetation: a discrete approach. IEEE Trans. Geosci. Remote Sens. 62–71.
Larson, K.M., Small, E.E., Gutmann, E.D., Bilich, A.L., Braun, J.J., Zavorotny, V.U., 2008. Use of GPS receivers as a soil moisture network for water cycle studies. Geophys. Res. Lett. 35.
Lee, J.H., Budhathoki, S., Lindenschmidt, K.-E., 2021. Stochastic bias correction for RADARSAT-2 soil moisture retrieved over vegetated areas. Geocarto International 1–14.
Lievens, H., Verhoest, N., De Keyser, E., Vernieuwe, H., Matgen, P., Álvarez-Mozos, J., De Baets, B., 2011. Effective roughness modelling as a tool for soil moisture retrieval from C-and L-band SAR. Hydrol. Earth Syst. Sci. Discuss. 7, 4995–5031.
Mattia, F., Satalino, G., Dente, L., Pasquariello, G., 2006. Using a priori information to improve soil moisture retrieval from ENVISAT ASAR AP data in semiarid regions. IEEE Trans. Geosci. Remote Sens. 44, 900–912.
Mattia, F., Satalino, G., Pauwels, V., Loew, A., 2009. Soil moisture retrieval through a merging of multi-temporal L-band SAR data and hydrologic modelling. Hydrol. Earth Syst. Sci. 13, 343–356.
Merlin, O., Walker, J., Panciera, R., Young, R., Kalma, J., Kim, E., 2007. Calibration of a soil moisture sensor in heterogeneous terrain. In: Oxley, L., Kulasiri, D. (Eds.), 2007 International Congress on Modelling and Simulation (MODSIM). Modelling and Simulation Society of Australia and New Zealand, pp. 2604–2610.
Merzouki, A., McNairn, H., 2015. A hybrid (Multi-angle and multi-Polarization) approach to soil moisture retrieval using the integral equation model: preparing for the RADARSAT constellation Mission. Can. J. Remote. Sens. 00.
Moghaddam, M., Silva, A., Clewley, D., Akbar, R., Hussaini, S., Whitcomb, J., Devarakonda, R., Shrestha, R., Cook, R., Prakash, G., 2016. Soil Moisture Profiles and Temperature Data from SoilSCAPE Sites, USA, ORNL DAAC, Oak Ridge, Tennessee, USA.
Neill, O.E., Chan, S., Njoku, E.G., Jackson, T., Bindlish, R., Chaubell, J., 2019. SMAP L3 Radiometer Global Daily 36 km EASE-Grid Soil Moisture. N.N.S.a.I.D.C.D.A.A. Center.
Njoku, E.G., Wilson, W.J., Yueh, S.H., Dinardo, S.J., Li, F.K., Jackson, T.J., Lakshmi, V., Bolten, J., 2002. Observations of soil moisture using a passive and active low-frequency microwave airborne sensor during SGP99. IEEE Trans. Geosci. Remote Sens. 40, 2659–2673.
Oh, Y., 2004. Quantitative retrieval of soil moisture content and surface roughness from multipolarized radar observations of bare soil surfaces. IEEE Trans. Geosci. Remote Sens. 42, 596–601.
Ojo, E.R., Bullock, P.R., L'Heureux, J., Powers, J., McNairn, H., Pacheco, A., 2015. Calibration and evaluation of a frequency domain reflectometry sensor for real-time soil moisture monitoring. Vadose Zone J. 14.
Ouellette, J.D., Johnson, J.T., Balenzano, A., Mattia, F., Satalino, G., Kim, S.-B., Dunbar, R.S., Colliander, A., Cosh, M.H., Caldwell, T.G., 2017. A time-series approach to estimating soil moisture from vegetated surfaces using L-band radar backscatter. IEEE Trans. Geosci. Remote Sens. 55, 3186–3193.
Palmisano, D., Mattia, F., Balenzano, A., Satalino, G., Pierdicca, N., Guarnieri, A.V.M., 2020. Sentinel-1 sensitivity to soil moisture at high incidence angle and the impact on retrieval over seasonal crops. IEEE Trans. Geosci. Remote Sens. 59, 7308–7321.
Peng, J., Albergel, C., Balenzano, A., Brocca, L., Cartus, O., Cosh, M.H., Crow, W.T., Dabrowska-Zielinska, K., Dadson, S., Davidson, M.W., 2020. A roadmap for high-resolution satellite soil moisture applications–confronting product characteristics with user requirements. Remote Sens. Environ. 112162.
Pierdicca, N., Castracane, P., Pulvirenti, L., 2008. Inversion of electromagnetic models for bare soil parameter estimation from multifrequency polarimetric SAR data. Sensors 8, 8181–8200.
Pierdicca, N., Pulvirenti, L., Bignami, C., 2010. Soil moisture estimation over vegetated terrains using multitemporal remote sensing data. Remote Sens. Environ. 114, 440–448.
Quegan, S., Le Toan, T., Chave, J., Dall, J., Exbrayat, J.-F., Minh, D.H.T., Lomas, M., D'alessandro, M.M., Paillou, P., Papathanassiou, K., 2019. The European Space Agency BIOMASS mission: measuring forest above-ground biomass from space. Remote Sens. Environ. 227, 44–60.
Rahman, M., Moran, M., Thoma, D., Bryant, R., Collins, C.H., Jackson, T., Orr, B., Tischler, M., 2008. Mapping surface roughness and soil moisture using multi-angle radar imagery without ancillary data. Remote Sens. Environ. 112, 391–402.
Sahebi, M., Angles, J., 2010. An inversion method based on multi-angular approaches for estimating bare soil surface parameters from RADARSAT-1. Hydrol. Earth Syst. Sci. 14, 2355–2366.
Schaefer, G.L., Cosh, M.H., Jackson, T.J., 2007. The USDA natural resources conservation service soil climate analysis network (SCAN). J. Atmos. Ocean. Technol. 24, 2073–2077.
Shi, H., Zhao, L., Yang, J., Lopez-Sanchez, J.M., Zhao, J., Sun, W., Shi, L., Li, P., 2021. Soil moisture retrieval over agricultural fields from L-band multi-incidence and multitemporal PolSAR observations using polarimetric decomposition techniques. Remote Sens. Environ. 261, 112485.
Shi, J., Wang, J., Hsu, A.Y., O'Neill, P.E., Engman, E.T., 1997. Estimation of bare surface soil moisture and surface roughness parameter using L-band SAR image data. IEEE Trans. Geosci. Remote Sens. 35, 1254–1266.
Smith, A., Walker, J., Western, A., Young, R., Ellett, K., Pipunic, R., Grayson, R., Siriwardena, L., Chiew, F., Richter, H., 2012. The Murrumbidgee soil moisture monitoring network data set. Water Resour. Res. 48.
Su, Z., Wen, J., Dente, L., Van Der Velde, R., Wang, L., Ma, Y., Yang, K., Hu, Z., 2011. The tibetan plateau observatory of plateau scale soil moisture and soil temperature (Tibet-Obs) for quantifying uncertainties in coarse resolution satellite and model products. Hydrol. Earth Syst. Sci. 15, 2303–2316.
Torres, R., Snoeij, P., Geudtner, D., Bibby, D., Davidson, M., Attema, E., Potin, P., Rommen, B., Floury, N., Brown, M., 2012. GMES Sentinel-1 mission. Remote Sens. Environ. 120, 9–24.
Ulaby, F.T., Long, D.G., Blackwell, W.J., Elachi, C., Fung, A.K., Ruf, C., Sarabandi, K., Zebker, H.A., Van Zyl, J., 2014. Microwave radar and radiometric remote sensing. The University of Michigan Press, Ann Arbor.
Verhoest, N., De Baets, B., Mattia, F., Satalino, G., Lucau, C., Defourny, P., 2007. A possibilistic approach to soil moisture retrieval from ERS synthetic aperture radar backscattering under soil roughness uncertainty. Water Resour. Res. 43.
Vernieuwe, H., Verhoest, N.E., Lievens, H., De Baets, B., 2010. Possibilistic soil roughness identification for uncertainty reduction on SAR-retrieved soil moisture. IEEE Trans. Geosci. Remote Sens. 49, 628–638.
Wagner, W., Lemoine, G., Borgeaud, M., Rott, H., 1999a. A study of vegetation cover effects on ERS scatterometer data. IEEE Trans. Geosci. Remote Sens. 37, 938–948.
Wagner, W., Lemoine, G., Rott, H., 1999b. A method for estimating soil moisture from ERS scatterometer and soil data. Remote Sens. Environ. 70, 191–207.
Wang, Z., Che, T., Zhao, T., Dai, L., Li, X., Wigneron, J.-P., 2021a. Evaluation of SMAP, SMOS, and AMSR2 soil moisture products based on distributed ground observation network in cold and arid regions of China. IEEE J. Sel. Top. Appl. Earth Obs. Remote Sens. 14, 8955–8970.
Wang, Z., Zhao, T., Qiu, J., Zhao, X., Li, R., Wang, S., 2021b. Microwave-based vegetation descriptors in the parameterization of water cloud model at L-band for soil moisture retrieval over croplands. GISci. Remote Sens. 58, 48–67.
Ye, N., Walker, J.P., Wu, X., Jeu, R.D., Gao, Y., Jackson, T.J., Jonard, F., Kim, E., Merlin, O., Pauwels, V., Renzullo, L.J., Rüdiger, C., Sabaghy, S.C., Hebel, V., Yueh, S. H., Zhu, L., 2020. The soil moisture active passive experiments: validation of the SMAP products in Australia. IEEE Trans. Geosci. Remote Sens. 59, 2922–2939.

Zhan, X., Houser, P.R., Walker, J.P., Crow, W.T., 2006. A method for retrieving high-resolution surface soil moisture from hydros L-band radiometer and radar observations. Geosci. Remote Sens. IEEE Trans. 44, 1534–1544.
Zhao, T., Shi, J., Entekhabi, D., Jackson, T.J., Hu, L., Peng, Z., Yao, P., Li, S., Kang, C.S., 2021. Retrievals of soil moisture and vegetation optical depth using a multi-channel collaborative algorithm. Remote Sens. Environ. 257, 112321.
Zhao, T., Shi, J., Lv, L., Xu, H., Chen, D., Cui, Q., Jackson, T.J., Yan, G., Jia, L., Chen, L., 2020. Soil moisture experiment in the Luan River supporting new satellite mission opportunities. Remote Sens. Environ. 240, 111680.
Zhu, L., Si, R., Shen, X., Walker, J., 2022. An advanced change detection method for time series soil moisture retrieval from Sentinel-1. Remote Sens. Environ. 279, 113137.
Zhu, L., Walker, J.P., Shen, X., 2020. Stochastic ensemble methods for multi-SAR-mission soil moisture retrieval. Remote Sens. Environ. 251, 112099.
Zhu, L., Walker, J.P., Tsang, L., Huang, H., Ye, N., Rüdiger, C., 2019a. A multi-frequency framework for soil moisture retrieval from time series radar data. Remote Sens. Environ. 235, 111433.
Zhu, L., Walker, J.P., Tsang, L., Huang, H., Ye, N., Rüdiger, C., 2019b. Soil moisture retrieval from time series multi-angular radar data using a dry down constraint. Remote Sens. Environ. 231, 111237.
Zhu, L., Walker, J.P., Ye, N., Rudiger, C., 2016. The effect of radar configuration on effective correlation length. In: Electromagnetics in Advanced Applications (ICEAA), 2016 International Conference on. IEEE, pp. 820–823.
Zribi, M., Foucras, M., Baghdadi, N., Demarty, J., Muddu, S., 2020. A new reflectivity index for the retrieval of surface soil moisture from radar data. IEEE J. Sel. Top. Appl. Earth Obs. Remote Sens. 14, 818–826.
Zribi, M., Gorrab, A., Baghdadi, N., 2014. A new soil roughness parameter for the modelling of radar backscattering over bare soil. Remote Sens. Environ. 152, 62–73.
Zribi, M., Saux-Picart, S., André, C., Descroix, L., Ottlé, C., Kallel, A., 2007. Soil moisture mapping based on ASAR/ENVISAT radar data over a sahelian region. Int. J. Remote Sens. 28, 3547–3565.